CONF-911003--27

ANL/CP--76452

DE92 016780

# Intrinsic Response of Crystals to Pure Dilatation

Jinghan Wang, Sidney Yip
Department of Nuclear Engineering
Massachusetts Institute of Technology, Cambridge, MA 02139

Simon Phillpot and Dieter Wolf
Materials Science Division
Argonne National Laboratory,* Argonne, IL 60439-4838



*Work supported by the U.S. Department of Energy, Office of Basic Energy Sciences-Materials Sciences, under Contract No. W-31-109-Eng-38.

INVITED PAPER presented at the Symposium on Solid State Amorphizing Transformations at TMS Fall Meeting, Cincinnati, Ohio, October 22-23, 1991.

# INTRINSIC RESPONSE OF CRYSTALS TO PURE DILATATION

Jinghan Wang[1], Sidney Yip[1], Simon Phillpot[2], and Dieter Wolf[2]

[1]Department of Nuclear Engineering, Massachusetts Institute of Technology, Cambridge, MA 02139

[2]Materials Science Division, Argonne National Laboratory, Argonne, IL 60439

## Abstract

The response of an f.c.c. lattice with Lennard-Jones interaction under symmetric lattice extension has been studied by Monte Carlo simulation at several temperatures. The critical strain at which the crystal undergoes a structural change is found to be well predicted by the mechanical stability limit expressed in terms of either the elastic constants or the bulk modulus. At low temperature (reduced temperature T = 0.125), lattice decohesion is observed in the form of cleavage fracture, whereas at higher temperature (T = 0.3) the strained system deforms by cavitation with some degree of local plasticity. At still higher temperature (T = 0.5) the lattice undergoes homogeneous disordering with all the attendant characteristics of melting.

Invited paper presented at the Symposium on Solid State Amorphizing Transformations, TMS Fall Meeting, Cincinnati, OH, October 22-23, 1991, for publication in a special issue of the Journal of Alloys and Compounds devoted to solid-state amorphization.

## I. Introduction

It is by now well established that solid-state amorphization (SSA), the process of crystal-to-glass transition, can be induced in intermetallic compounds by various perturbations ranging from particle beam irradiations, chemical reactions, to mechanical deformations.[1-3] A fundamental question which still remains concerns the underlying nature of the transition and the relative importance of the effects of point defects, chemical disorder, and other possible driving forces for lattice destabilization. Following the observation that structural disordering in all cases is accompanied by a volume expansion [2], it has been suggested that role of local density variations in SSA may be analogous to that in the melting transition.[4] The implication is that at temperatures below the triple point, essentially the melting point at zero pressure $T_m$, a sudden volume expansion (on the time scale short compared to that required for equilibrium sublimation) may bring about structural disordering.

In this paper we report the results of Monte Carlo simulation of the structural response of an f.c.c. crystal to pure dilatation imposed at constant temperatures. The purpose of the study is to test the prediction of lattice instability based on elastic-constant criteria and to determine by direct observation whether crystal disordering can be induced by symmetric lattice extension. Using the Lennard-Jones potential to model the interatomic interaction, we find that the critical strain at which structural change occurs is well predicted by the mechanical stability limits. At low temperature (reduced temperature T = 0.125) anisotropic lattice decohesion occurs at the critical strain and overall the system remains crystalline. At higher temperature (T = 0.3) cavitation-like local

deformation occurs with indications of anisotropic disordering. At still higher temperature (T = 0.5) the lattice disorders uniformly with all the characteristics of melting.

## II. Simulation Model and Procedure

The simulation system is a cubic cell of N particles arranged on an f.c.c. lattice. The particles interact with each other through a Lennard-Jones (6-12) potential which is truncated at a distance $R_c$ and shifted to zero at the cutoff. The cell is periodic in all three directions. In each simulation run at a certain temperature, the lattice parameter a is held fixed while the particles are allowed to move by Monte Carlo.[5] The process is then repeated at an incrementally larger a. Typically the first 10,000 moves per particle are discarded as equilibration, and another 30,000 moves per particle are made to accumulate the configurations for property calculations. All quantities reported below will be expressed in reduced units where length and energy are scaled by the parameters $\sigma$ and $\epsilon$ of the potential.

Simulation of strain-induced response has been carried out at the temperatures T = 0.125, 0.3, 0.5, and 0.8. (As a reference, for the Lennard-Jones potential $T_m$ can be taken to be 0.61.[6]) Most of the runs were made with a cell of 500 particles, but runs using N = 108 and 864 were also performed to give some indications of system size effects. In all the runs the value of $R_c$ is 2.3273.

III. Pressure and Potential Energy Responses

Fig. 1 shows the variation at T = 0.3 of the hydrostatic pressure, calculated using the virial expression [7], as the lattice parameter a of the f.c.c. cell is increased incrementally. Starting at a value of the lattice parameter which gives zero pressure, the system is seen to go into negative pressure as isotropic strain is imposed. This negative pressure increases monotonically and appears to level off at a maximum value. With further lattice dilatation the pressure first decreases somewhat and then jumps abruptly to a considerably reduced though still finite value. The N=500 data show this characteristic behavior quite clearly. The data for N=864 are quite consistent with these results, whereas the onset of the abrupt change in the small system, N = 108, occurs at a somewhat larger value of strain.

Fig. 2 shows the potential energy of the system in response to isotropic strain. As the lattice goes into negative pressure, more and more strain energy is stored in the system. This continues until the pressure changes suddenly (cf. Fig. 1), at which point the potential energy drops correspondingly. Again, the N=864 data are consistent with the N=500 results, whereas for N=108 the decrease in potential energy occurs at higher strain and is barely discernible.

The existance of a critical value of imposed strain, as indicated in Figs. 1 and 2, suggests the onset of a structural transition which we will investigate in the following by examining directly the atomic configurations produced at each incremental strain. As for the nature of the transition, one can ask what is the connection between the behavior observed in Fig. 1 and the mechanical stability limit which one can derive

for a uniform lattice. We have already noted that the tension appears to reach a maximum value at a lattice parameter which we will denote as $a_c$, and that $a_c$ is distincly smaller than the critical value at which the pressure jumps suddenly which we will denote by $a_p$. Since we have results for three system sizes, we can perform a 1/N extrapolation on the value of $a_p$ as directly observed in the simulation data. This gives a critical strain of $\epsilon_p = (a_p - a_o)/a_o = 0.0687$. To determine $\epsilon_c$, we fit for each N the several data points for the pressure in the vicinity of $a_c$ to a polynomial, and calculate dp/da = 0 from the fit. After a similar 1/N extrapolation we obtain $\epsilon_c = 0.0628$. The apparent discrepancy between $\epsilon_p$ and $\epsilon_c$ is believed not to be significant given the large fluctuations in the system pressure in the region of the critical behavior, and the fact that system size effects may not have been fully eliminated in our 1/N-extrapolation based on limited data.

## IV. Elastic Constants

Returning to the question of intrinsic mechanical stability limit, we have determined the elastic constants of a cubic lattice by applying the fluctuation formula derived by Ray, Moody, and Rahman [8] for a stressed solid. In the case of uniform strain, the adiabatic elastic constant $C_{ijk\ell}$ is given by

$$C_{ijk\ell} = (\ell_o/\ell)\Big[ - \frac{V}{k_B T}\,\delta(P_{ij}P_{k\ell}) + \frac{2Nk_BT}{V}(\delta_{i\ell}\delta_{jk} + \delta_{ik}\delta_{j\ell}) + \frac{1}{V} < \sum_{b>a} f(r_{ab}) x_{abi} x_{abj} x_{abk} x_{ab\ell} > \Big] \qquad (1)$$

where

$$f(r) = r^{-2}[d^2u(r)/dr^2 - \chi(r)] \qquad (2)$$

$$P_{ij} = \frac{1}{V}\left[\sum_{a} p_{ai}p_{aj}/m - \sum_{b>a} \chi(r_{ab})x_{abi}x_{abj}\right] \qquad (3)$$

and $\chi(r) = [du(r)/dr]/r$, with $u(r)$ being the interatomic potential function. In Eq.(1) $\ell_o$ and $\ell$ are the lengths of the simulation cell before and after the imposed strain respectively, V is the volume of the strained cell which contains N particles, and $\langle\ \rangle$ denotes an ensemble average. In addition, $r_{ab}$ is the separation distance between particles a and b, and $x_{abi}$ is the ith Cartesian component of the vector $\underline{r}_{ab}$. In Eq.(3) $p_{ai}$ is a momentum component and m the particle mass, thus $P_{ij}$ is the stress tensor.

Applying Eq.(1) to the atomic configurations generated by the Monte Carlo runs, we have computed the three elastic constants $C_{11}$, $C_{12}$, and $C_{44}$. For a lattice to be mechanically stable one can show that the inequalities,

$$C_{11} > 0, \quad C_{11} - C_{12} > 0, \quad C_{44} > 0 \qquad (4)$$

must hold [9], along with $C_{12} > 0$ ,arising from the physical condition that the Poisson ratio must be greater than zero [10]. These criteria may be compared to the requirement of positive isothermal bulk modulus $B_T = -V(\partial P/\partial V)_T$, a thermodynamic condition. Our elastic constant results at T = 0.3 and different system sizes are shown in Fig. 3. It can be seen that all three elastic constants have decreased to quite small values in the region of the critical strain. The elastic constants behave normally while they are still positive, but once an elastic constant has reached zero value, subsequent behavior at still larger strain shows unphysical oscillations. The first term in Eq.(1) represents the effects of stress tensor

fluctuations. In the critical-strain region it is large and fluctuates strongly, thus giving rise to appreciable uncertainties in the calculated elastic constants. As a result we can only say that as $C_{11}$ approaches $C_{12}$, both appear to be approaching zero. At the same time, the data suggest that $C_{44}$ remains finite at the critical strain. Within the estimated statistical error the mechanical stability limit seems to be consistent with $\epsilon_c$.

## V. Structural Responses

The onset of a sudden change in the pressure and potential change is an indication that an accompanying structural change must have also occurred. The above consideration of mechanical stability, while useful for determining the critical strain at which ths change takes place, tells us nothing about the state into which the system evolves. For this information it is necessary to examine the atomic configurations at various stages of strain.

We will characterize the atomic configurations in terms of the radial distribution function g(r) [7] which provides a measure of local spatial correlation, without specification of direction, and the corresponding quantity the static structure factor $S(\underline{k})$, with $\underline{k}$ being a wave vector. By computing $S(\underline{k})$ for a large number of suitably chosen $\underline{k}$, one can generate a diffraction pattern which provides a measure of direction-dependent structural order in the system.

Fig. 4 shows the g(r) and $S(\underline{k})$ results for the T = 0.3 runs with N = 500 at three values of the lattice parameter a, $a = a_1 = 1.707$ specifies the system strain just before the pressure jump (cf. Fig. 1), $a = a_2 =$

1.723 is the value after two strain increments, and $a = a_3 = 1.747$ is the last dilatation imposed in this series. First we notice that in all three cases the g(r) results are quite similar, in particular a distinct peak can be seen at $r \sim 1.7$, the characteristic second-neighbor shell of the f.c.c. lattice. The corresponding diffraction patterns all display high intensity in the region around $k_x \sim k_y \sim 1$, as one would expect for the f.c.c. lattice. However, whereas the diffraction pattern at $a_1$ is quite symmetric, an assymetry along $k_x$ and $k_y$ about the Bragg position $k_x = k_y = 1$ can be noticed at $a_2$ and $a_3$.

More detailed information on the structural change in going from $a_1$ to $a_2$ and $a_3$ is provided by the density profiles given in Figs. 5 - 7. One sees that at $a_1$ the atomic planes along each direction of cubic symmetry are well ordered as in a perfect (undeformed) lattice. At $a_2$, after the pressure jump, symmetry is clearly broken in the y-direction; there appears an extra atomic plane along this direction, and moreover the system is no longer uniform along this direction. Another feature that can be seen in Fig. 6 is the distincly nonzero value of the minima in the density profiles which implies significant atomic displacements from the original lattice positions. In going from $a_2$ to $a_3$ (Fig. 7) the density profile along the y-direction shows two extra planes relative to the x- and z-directions. We interpret this as a tendency to change from cubic to tetragonal structure. Also the nonuniform density profiles along the x- and y-directions suggest the nucleation of cavitation, first seen in Fig. 6 along the y-direction.

One may ask whether further structural changes will take place if the dilatation were increased further. In the series of simulation at $T = 0.3$ using the $N = 864$ system, we have taken the system out to larger values of the lattice parameter as shown in Fig. 8. Up to approximately the same

value of $a = a_3$, the observed behavior is similar to the N = 500 data shown in Figs. 4 – 7. When the imposed strain is increased to $a_4 = 1.750$ and $a_5 = 1.757$, the density profiles, given in Figs. 9 and 10, show (i) pronounced cavitiation along the direction of broken symmetry (x–direction in this N = 864 series in contrast to y–direction in N = 500 series), and (ii) increasing loss of well–ordered planar structure along the cubic directions of the original lattice. It is interesting that the structural deformations which are clearly indicated by the density profiles do not give rise to any characteristic features in the g(r) and $S(\underline{k})$ results in Fig. 8, aside from an indication of assymetry in the latter.

The structural response at T = 0.125 generally are similar to those just presented at T = 0.3. The pressure and potential energy responses show the same jump behavior as in Figs. 1 and 2. The onset of cavitation is quite clearly seen, and as the system is further dilated, decohesion of the lattice planes occurs along a broken–symmetry direction.

The structural response at T = 0.5, on the other hand, is quite different from that at T = 0.3. Fig. 11 shows a pressure jump at the critical strain, but now the corresponding potential energy change is an increase instead of a decrease as in Fig. 2. Examination of g(r), $S(\underline{k})$ and density profiles at the strain after the pressure jump shows clearly the system has become completely disordered. It is also noteworthy that the mean–squared–displacement function evaluated at the strain before and after the pressure jump, given in Fig. 12, shows dramatically different mobility behavior over the same number of Monte Carlo sweeps. The essentially linear variation of the mean–squared–displacement and the increased magnitude of this quantity observed after the jump are strong indications of a liquid–like environment.

## VI. Discussion

In this work we have determined by Monte Carlo simulation and elastic constant calculations the structural stability limit of an f.c.c. Lennard-Jones lattice under symmetric isothermal extension along the three directions of initial cubic symmetry. We have shown that at several temperatures the critical strain is determined by the Born criteria involving the elastic constants. The values of these strains define a stability curve in the temperature–density phase diagram as shown in Fig. 13. It has been suggested that the freezing curve which, like the melting curve, is defined only for temperatures above the triple point $T_t$, is effectively also the mechanical stability curve in the sense of heating a crystal rapidly up to the limit of superheating.[4] It can be seen in Fig. 13 that the critical strains observed in the present work delineate the extension of the mechanical stability curve to temperatures below $T_t$. It has been conjectured that in crossing this stability curve the lattice will become disordered, thus providing a simple thermodynamic connection between melting and solid-state amorphization.[4] What we have found is that in crossing such a curve the lattice does become mechanically unstable as manifested by sudden jumps in the hydrostatic pressure and the potential energy; however, the atomic configuration into which it evolves depends on the temperature. The instability is accompanied by symmetry breaking as shown clearly by the density profiles along the three cubic directions. At the same time, the system becomes nonuniform by the formation of a local region of relatively low density. We interpret this crystal response as cavitation which at $T = 0.125$ ($0.18\ T_t$) leads to cleavage fracture upon further lattice dilatation. At $T = 0.3$ ($0.44\ T_t$), in addition to cavitation-like behavior, significant local disordering occurs as the

system is strained beyond the instability. At T = 0.5 (0.74 $T_t$) the system response at the instability is homogeneous and complete disordering as in a melting transition.

Regarding the question of whether pure volume expansion is sufficient to give rise to a crystal-to-amorphous transition, it appears that the present results on the Lennard-Jones system do not give a definitive answer. We feel that part of the problem stems from the relatively shallow well-depth of the potential as compared to an EAM-type potential [12] for metals. Thus the Lennard-Jones potential gives considerably lower values for the elastic constants which makes it difficult to distinguish between the criteria given by Eq.(4) and $C_{12} > 0$. A study is underway using an EAM potential for f.c.c. metal to see the influence of potential function details on the structural response to imposed strain.

As far as equation of state behavior is concerned, we can compare the Lennard-Jones system with the universal binding energy model [13], a simple two-parameter empirical description of the variation of the cohesive energy (the potential energy at zero temperature) with lattice parameter. According to this model, $E(a) = \Delta E\, E^*(a^*)$, with

$$E^*(a^*) = -\,(1 + a^* + 0.05\, a^{*3})\, e^{-a^*} \qquad (5)$$

where $\Delta E$ is the minimum value of the cohesive energy and $a^* = (a - a_E)/\ell$, $a_E$ being the lattice parameter at which the cohesive energy is a minimum and $\ell$ is a length scale which can be determined from the bulk modulus.[13] are the scaled energy and lattice parameter. Fig. 14(a) shows the

comparison between the Lennard-Jones result and Eq.(5). Given E(a) one can find the pressure at zero temperature from P = – dE/dV,

$$P(V) = 3B[(V/V_o)^{1/3}-1](V/V_o)^{-2/3}(1 - 0.15a^* + 0.05a^{*2})\ e^{-a^*} \qquad (6)$$

where B is the bulk modulus and $V_o = 4\pi a_E^3/3$. The comparison of the pressure calculated directly for the Lennard-Jones lattice with Eq.(6) is shown in Fig. 14(b). Taken together with Fig. 14(a) they show how well the Lennard-Jones system can be described by the simple analytic expressions given by the universal binding energy model, a description which has been found useful for metals. To see the effects of temperature we show in Fig. 15 the pressure variation in the vicinity of the critical strain obtained from the Monte Carlo simulation at T = 0.125 and the zero-temperature variation given by Eq.(6). The absence of a pressure jump in the latter clearly underscores the role of thermal fluctuations in symmetry breaking and initiation of structural deformation.

Acknowledgments

Work of JW and SY has been supported in part by a National Science Foundation Grant CHE-8806767, and by the Materials Science Division at the Argonne National Laboratory. Work of SP and DW was supported the U.S. Department of Energy BES-Materials Science under Contract No. W-31-109-Eng-38. Support for computational resources also has been provided by an allocation from the San Diego Supercomputer Center.

## References


1. For an overview see, W. L. Johnson, Prog. Mater. Sci. 30, 81 (1986), D. E. Luzzi and M. Meshii, Res. Mechanica 21, 207 (1987), and papers in J. Less-Comm. Met. 140 (1988).
2. P. R. Okamoto and M. Meshii, in Science of Advanced Materials, H. Wiedersich and M. Meshii, eds. (ASM International, Materials Park, OH, 1990), p.33.
3. W. L. Johnson, in Materials Interfaces – Atomic-Level Structure and Properties, D. Wolf and S. Yip, eds. (Chapman and Hall, London, 1992), to be published.
4. D. Wolf, P. R. Okamoto, S. Yip, J. F. Lutsko, M. Kluge, J. Mater. Res. 5, 286 (1990).
5. N. Metropolis, A. W. Rosenbluth, M. N. Rosenbluth, A. H. Teller, E. Teller, J. Chem. Phys. 21, 1087 (1953).
6. J. Q. Broughton and G. H. Gilmer, J. Chem. Phys. 79, 5095 (1983).
7. M. P. Allen and D. J. Tildesley, Computer Simulation of Liquids, (Clarendon, Oxford, 1987).
8. J. R. Ray, M. C. Moody, A. Rahman, Phys. Rev. B 32, 733 (1985).
9. M. Born, Proc. Cambridge Philos. Soc. 36, 160 (1940); F. Milstein and R. Hill, Phys. Rev. Lett. 43, 1411 (1979).
10. L. D. Landau and E. M. Lifshitz, Theory of Elasticity (Pergamon Press, Oxford, 1959), p. 14.
11. W. G. Hoover and W. T. Ashurst, in Theoretical Chemistry, – Advances and Perspectives, (Academic Press, New York, 1975), vol 1, p. 1.
12. M. S. Daw and M. I. Baskes, Phys. Rev. B 29, 6443 (1984).
13. J. H. Rose, J. R. Smith, F. Guinea, J. Ferrante, Phys. Rev. B 29, 2963 (1984).

## Figure Captions

Fig. 1. Variation of hydrostatic pressure with lattice parameter a at T = 0.3, N = 108 (triangles), 500 (circles), 864 (squares).

Fig. 2. Same as Fig. 1 except variation is that of the potential energy.

Fig. 3. Variations of the elastic constants, $C_{11}$ (a), $C_{12}$ (b), $C_{44}$ (c), with lattice parameter a at T = 0.3, N = 108 (triangles), 500 (circles), 864 (squares).

Fig. 4. System responses, g(r) and diffraction pattern $S(\underline{k})$ at T = 0.3, N = 500, and three values of lattice paramter, a = 1.707 (a), a = 1.723 (b), and a = 1.747 (c). $S(\underline{k})$ is shown in the inset as projections on $k_x$ (horizontal axis) and $k_y$(vertical axis).

Fig. 5. Density profiles corresponding to Fig. 4(a).

Fig. 6. Density profiles corresponding to Fig. 4(b).

Fig. 7. Density profiles corresponding to Fig. 4(c).

Fig. 8. Same as Fig. 4 except N = 864 and the two lattice parameter values are a = 1.750 (a), and a = 1.757 (b).

Fig. 9. Desnity profiles corresponding to Fig. 8(a).

Fig. 10. Desnity profiles corresponding to Fig. 8(b).

Fig. 11. System responses at T = 0.5 and N = 500, pressure (a) and potential energy (b). Note similarity with Fig. 1 in the pressure and difference from Fig. 2 in the potential energy.

Fig. 12. Variation of mean-squared-displacement function with Monte Carlo sweeps at two system strain states, just before (a) and just after (b) the pressure jump shown in Fig. 11. Note difference in scale of the ordinate axis.

Fig. 13. Temperature–volume phase diagram of an atomic system in which the particles interact via the Lennard–Jones potential function [11]. Critical strains, converted to densities, observed in the present simulation are added as circles at the various temperatures.

Fig. 14. Comparison of the cohesive energy (a) and pressure–volume relation (b) of the Lennard–Jones crystal at zero temperature (solid curve) with the universal binding energy model (dashed curve). Procedure used in scaling the lattice parameter and energy is discussed in the text.

Fig. 15. Pressure–volume relation of the Lennard–Jones crystal at T = 0.125 (solid curve) showing a jump which is absent in the universal binding energy model (dashed curve, same result as in Fig. 14 but on a different scale).

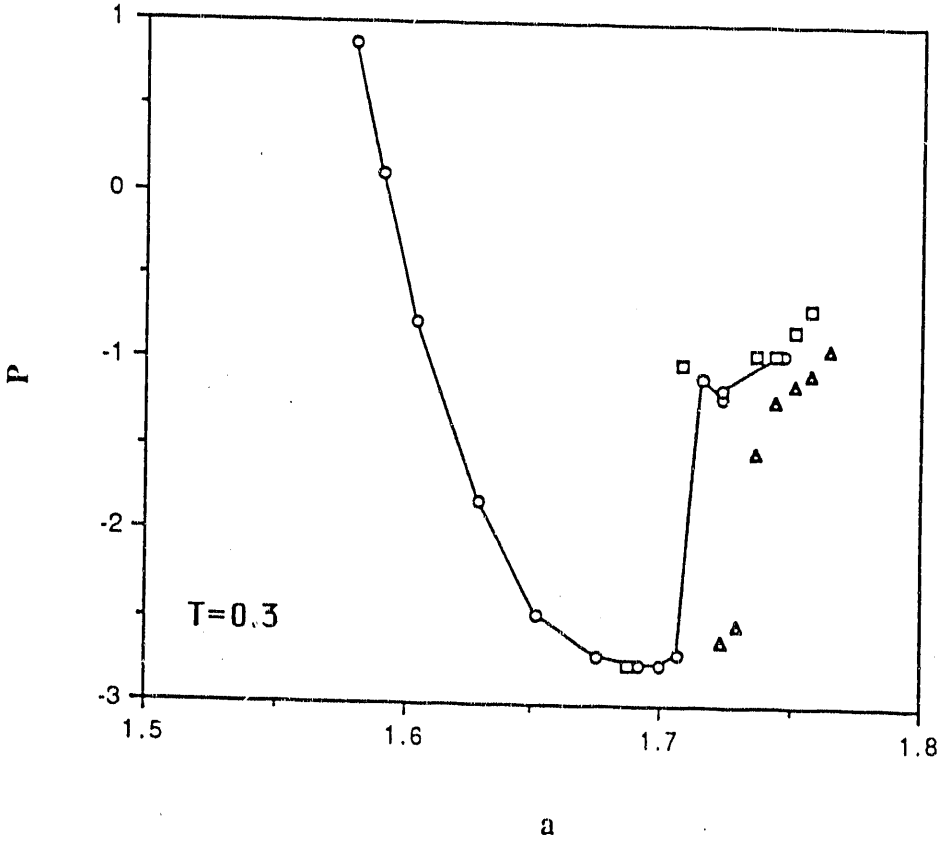


Fig. 1

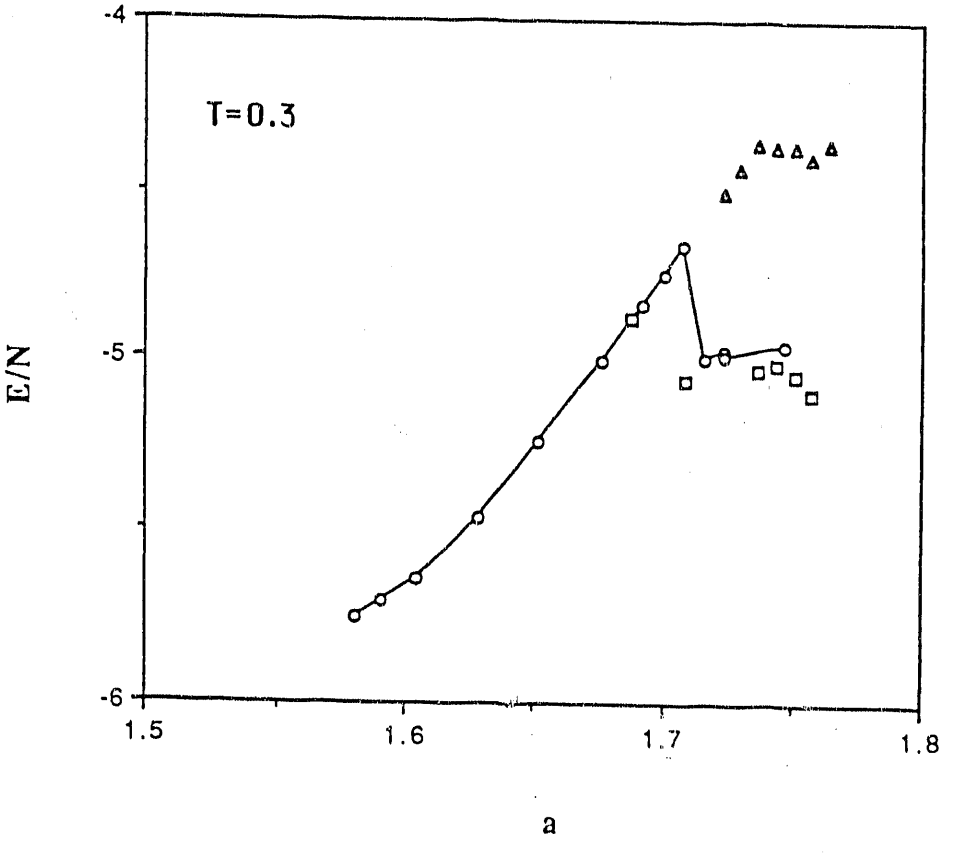


Fig. 2

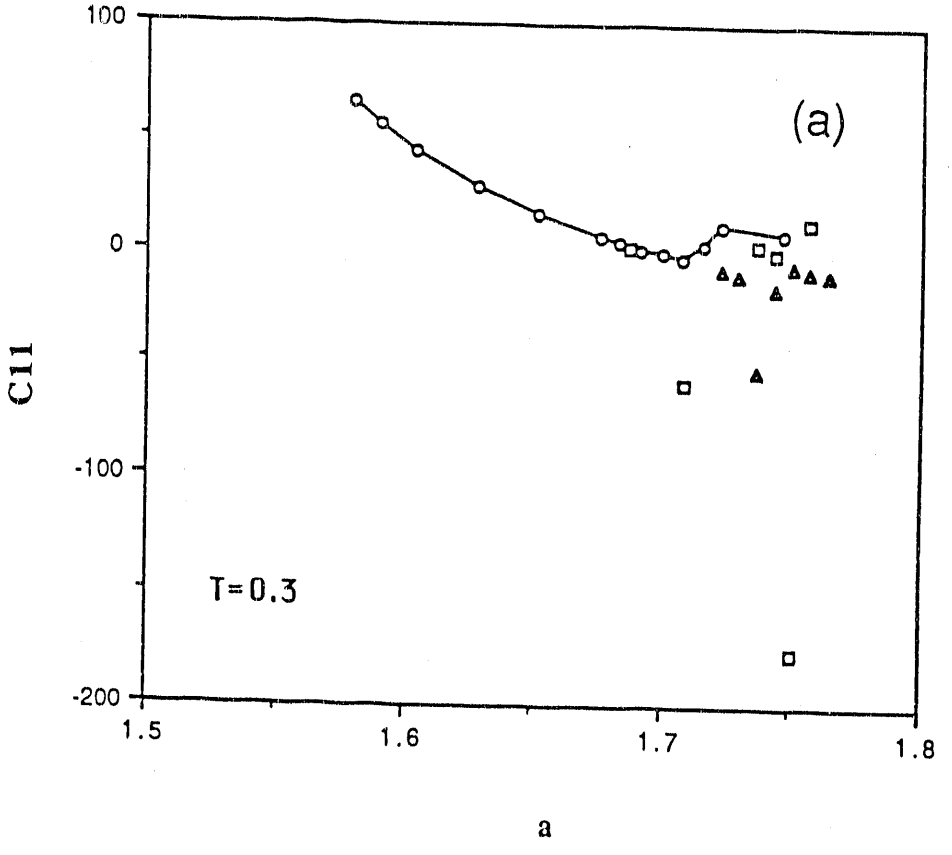


Fig. 3(a)

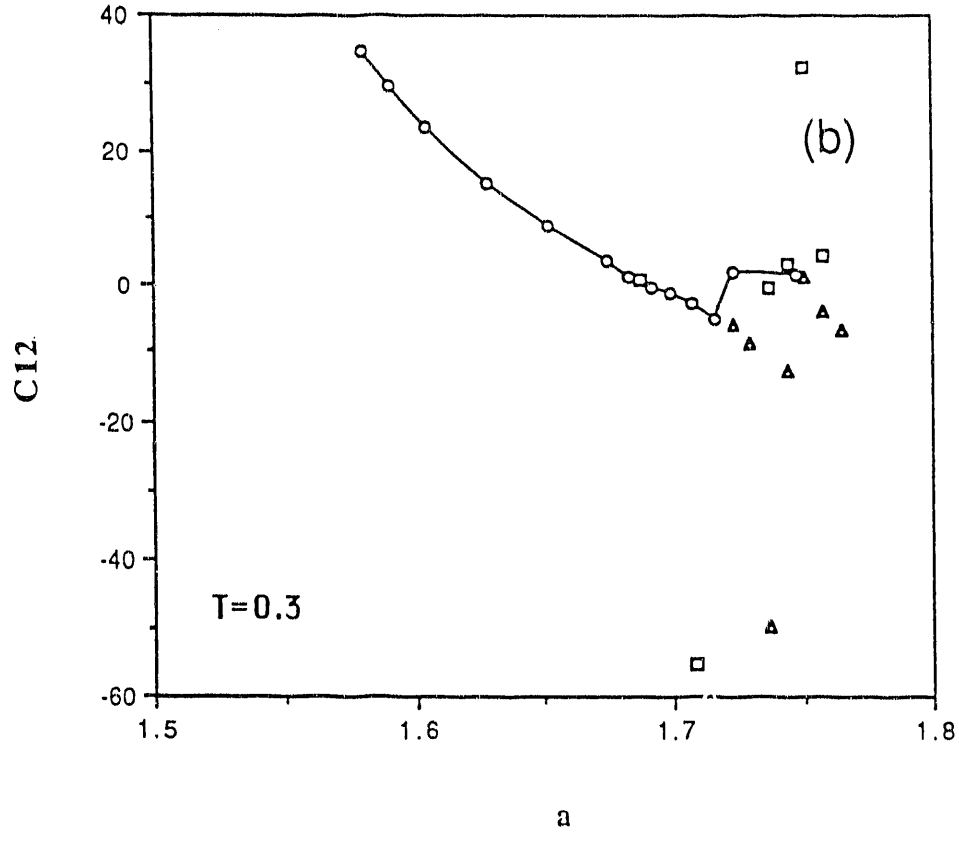


Fig. 3(b)

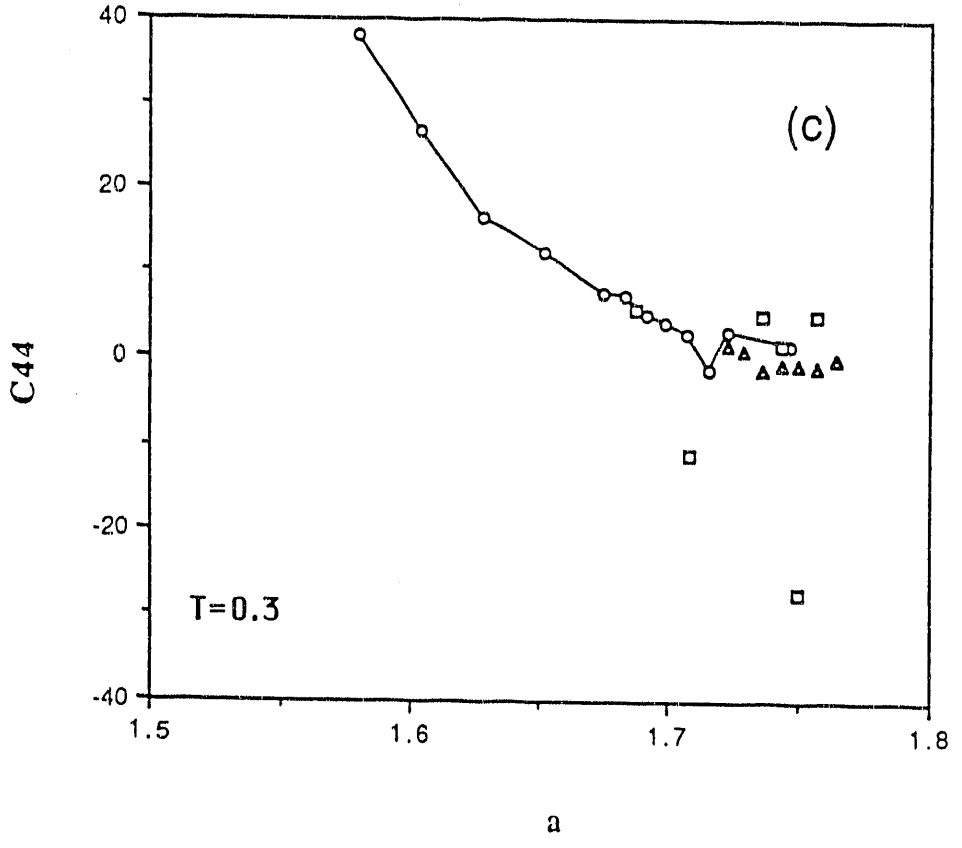


Fig. 3(c)

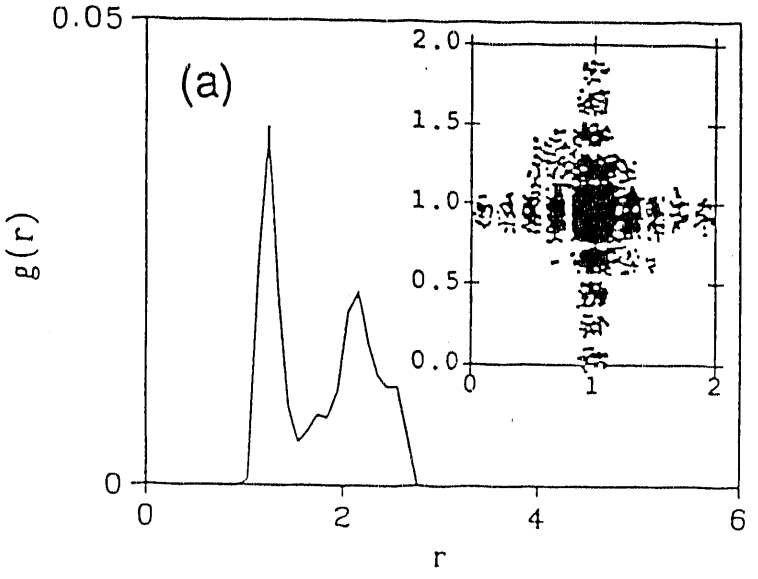
0.05
(a)
g(r)
0
0
2
4
6
r
2.0
1.5
1.0
0.5
0.0
0
1
2

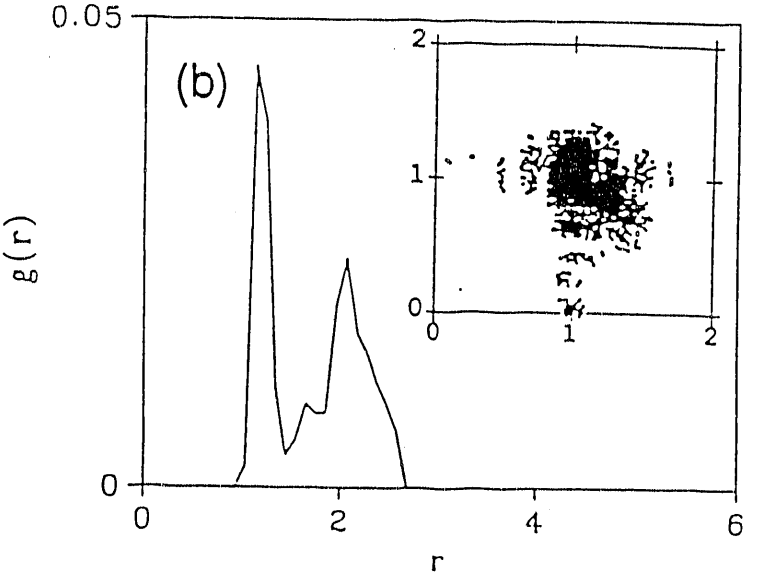
0.05
(b)
g(r)
0
0
2
4
6
r
2
1
0
0
1
2

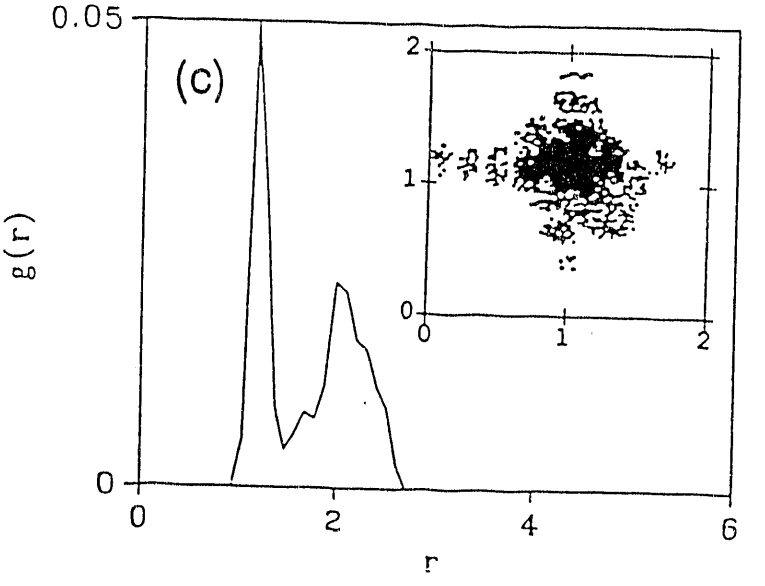
0.05
(c)
g(r)
0
0
2
4
6
r
2
1
0
0
1
2

Fig. 4

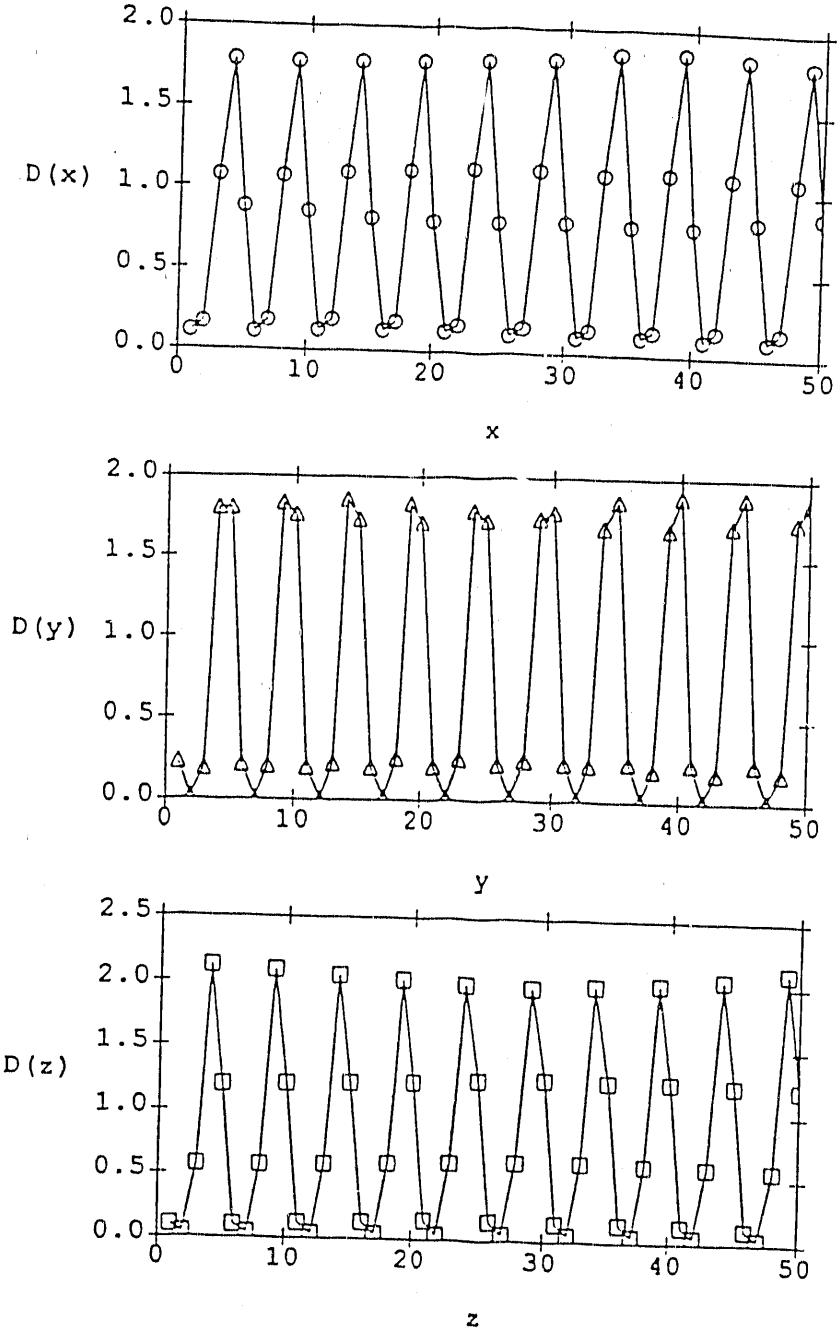
D(x)
2.0
1.5
1.0
0.5
0.0
0
10
20
30
40
50
x
D(y)
2.0
1.5
1.0
0.5
0.0
0
10
20
30
40
50
y
D(z)
2.5
2.0
1.5
1.0
0.5
0.0
0
10
20
30
40
50
z

Fig. 5

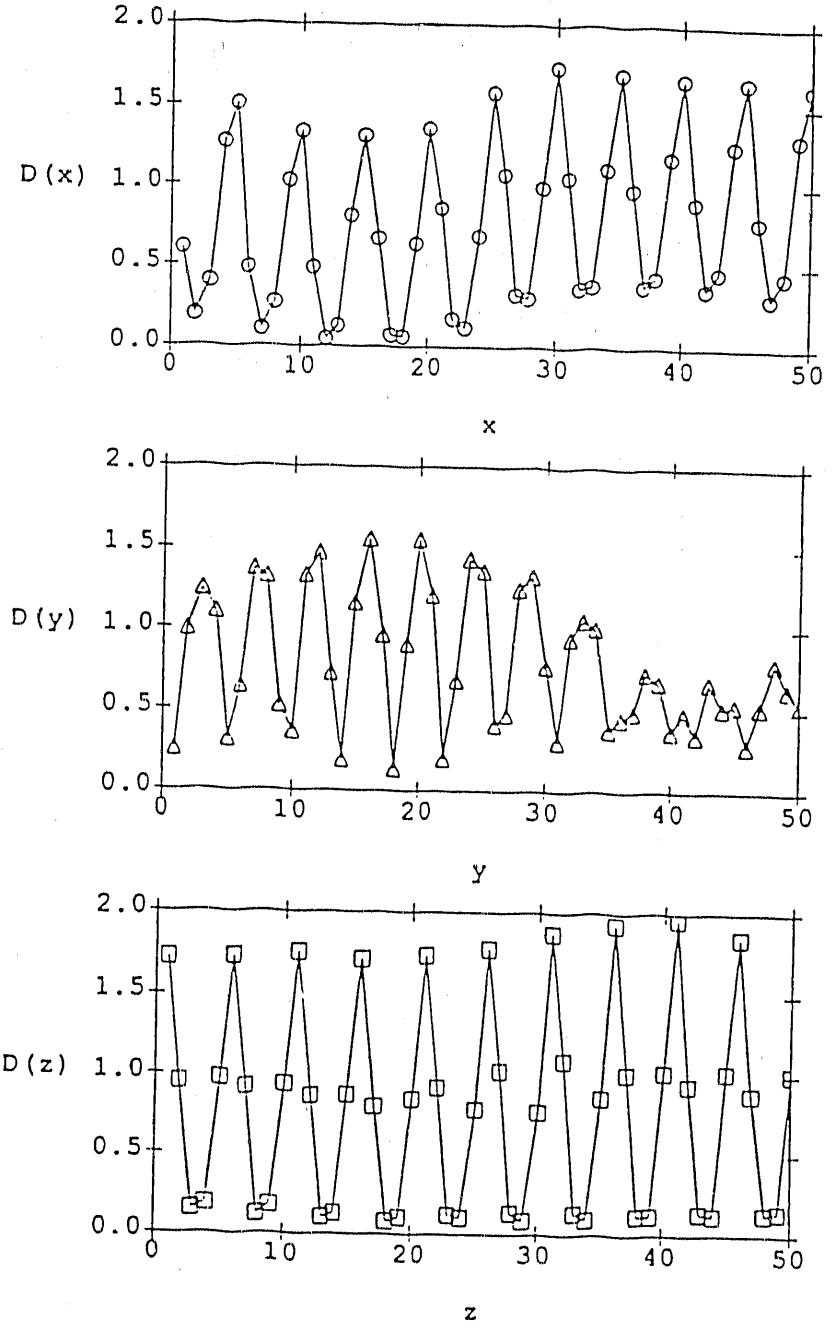
D(x)
2.0
1.5
1.0
0.5
0.0
0
10
20
30
40
50
x
D(y)
2.0
1.5
1.0
0.5
0.0
0
10
20
30
40
50
y
D(z)
2.0
1.5
1.0
0.5
0.0
0
10
20
30
40
50
z

Fig. 6

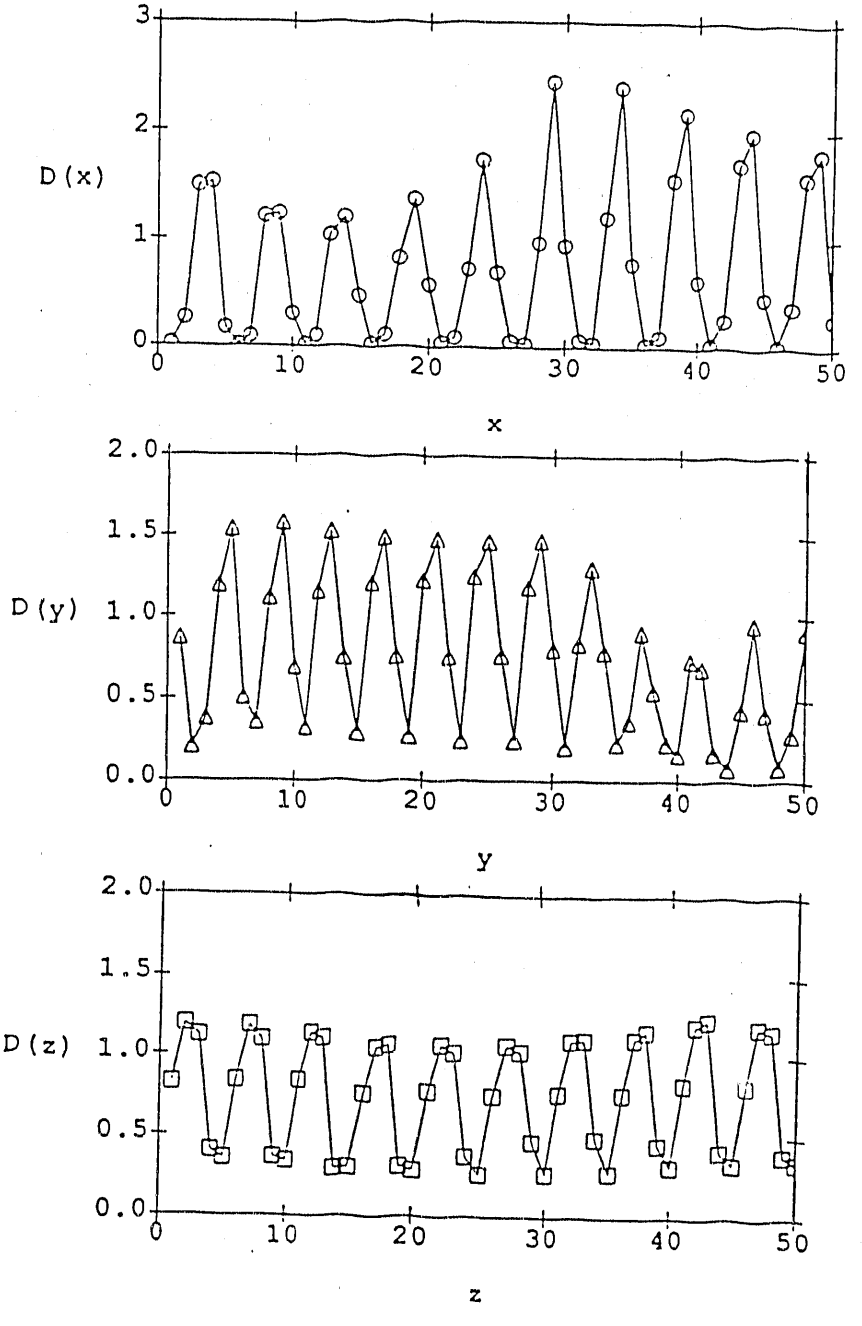
D(x)
3
2
1
0
0
10
20
30
40
50
x
D(y)
2.0
1.5
1.0
0.5
0.0
0
10
20
30
40
50
y
D(z)
2.0
1.5
1.0
0.5
0.0
0
10
20
30
40
50
z

Fig. 7

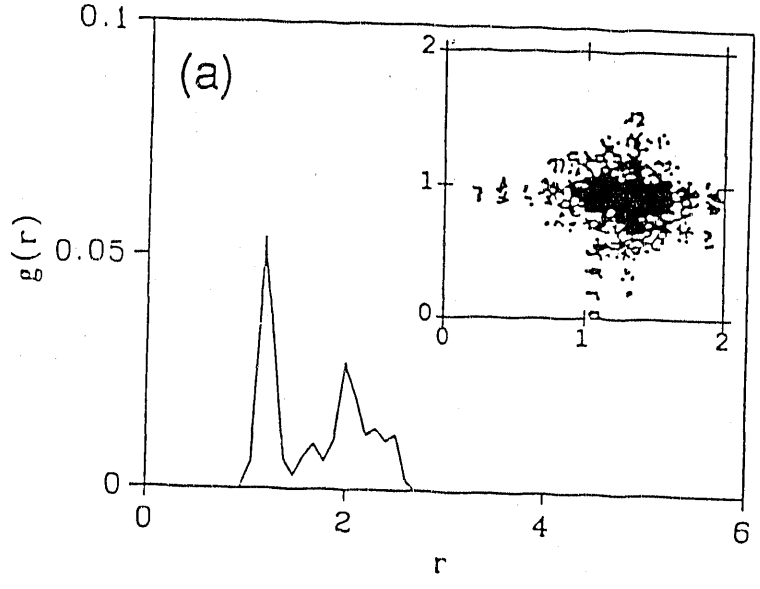
(a)
0.1
0.05
0
g(r)
0
2
4
6
r
2
1
0
0
1
2

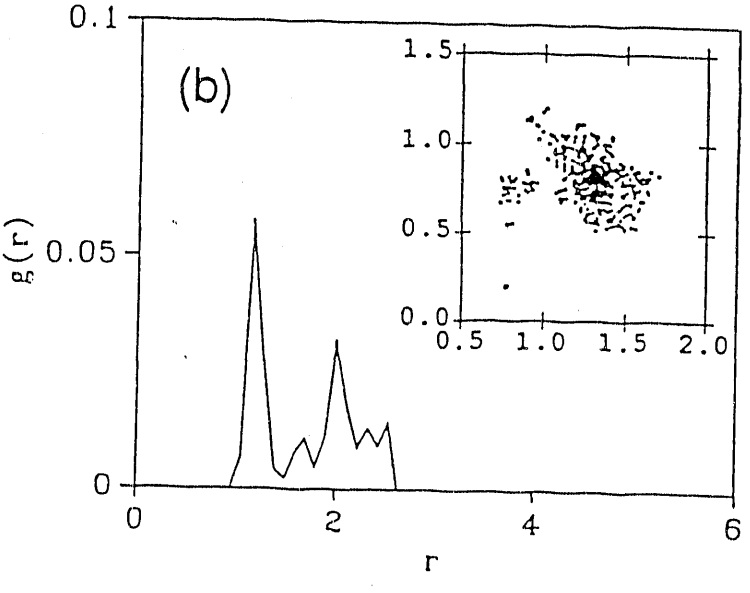
(b)
0.1
0.05
0
g(r)
0
2
4
6
r
1.5
1.0
0.5
0.0
0.5
1.0
1.5
2.0

Fig. 8

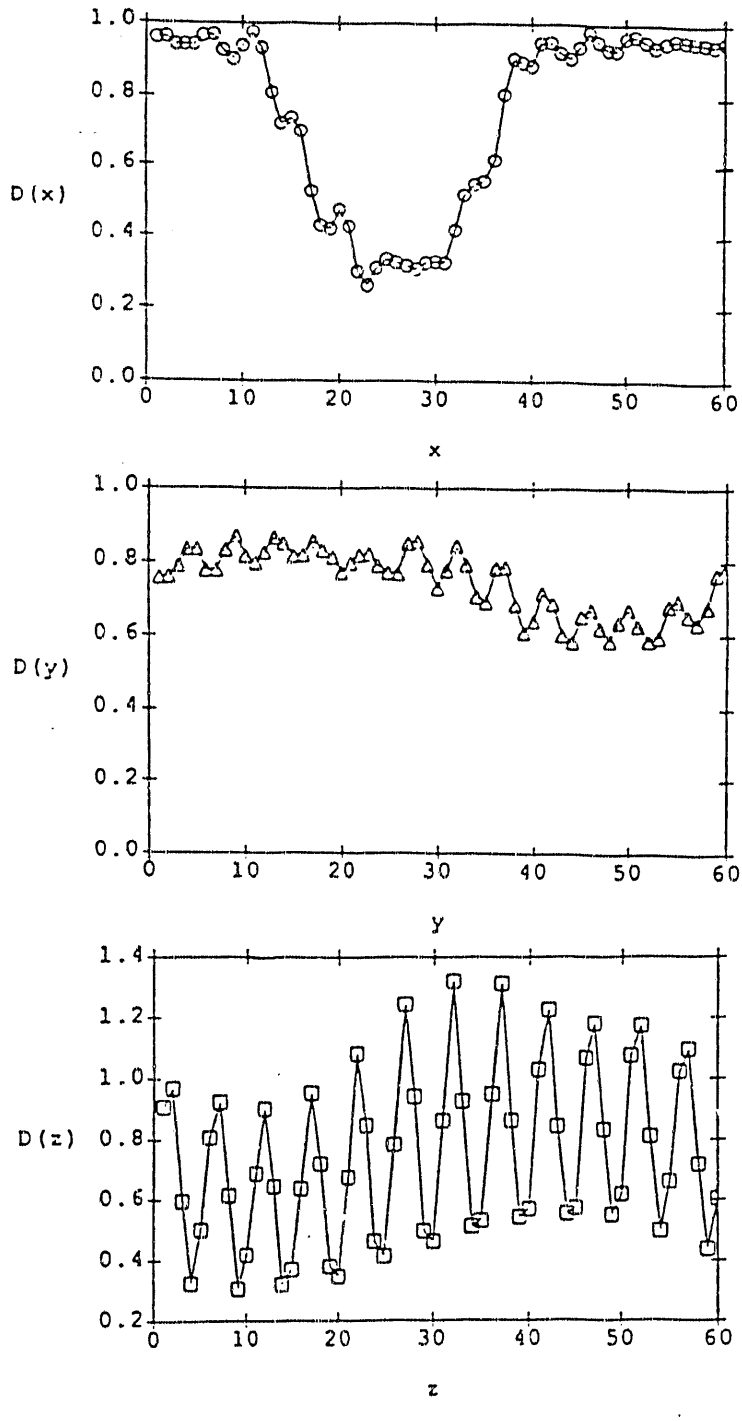
D(x)
1.0
0.8
0.6
0.4
0.2
0.0
0
10
20
30
40
50
60
x
D(y)
1.0
0.8
0.6
0.4
0.2
0.0
0
10
20
30
40
50
60
y
D(z)
1.4
1.2
1.0
0.8
0.6
0.4
0.2
0
10
20
30
40
50
60
z

Fig. 9

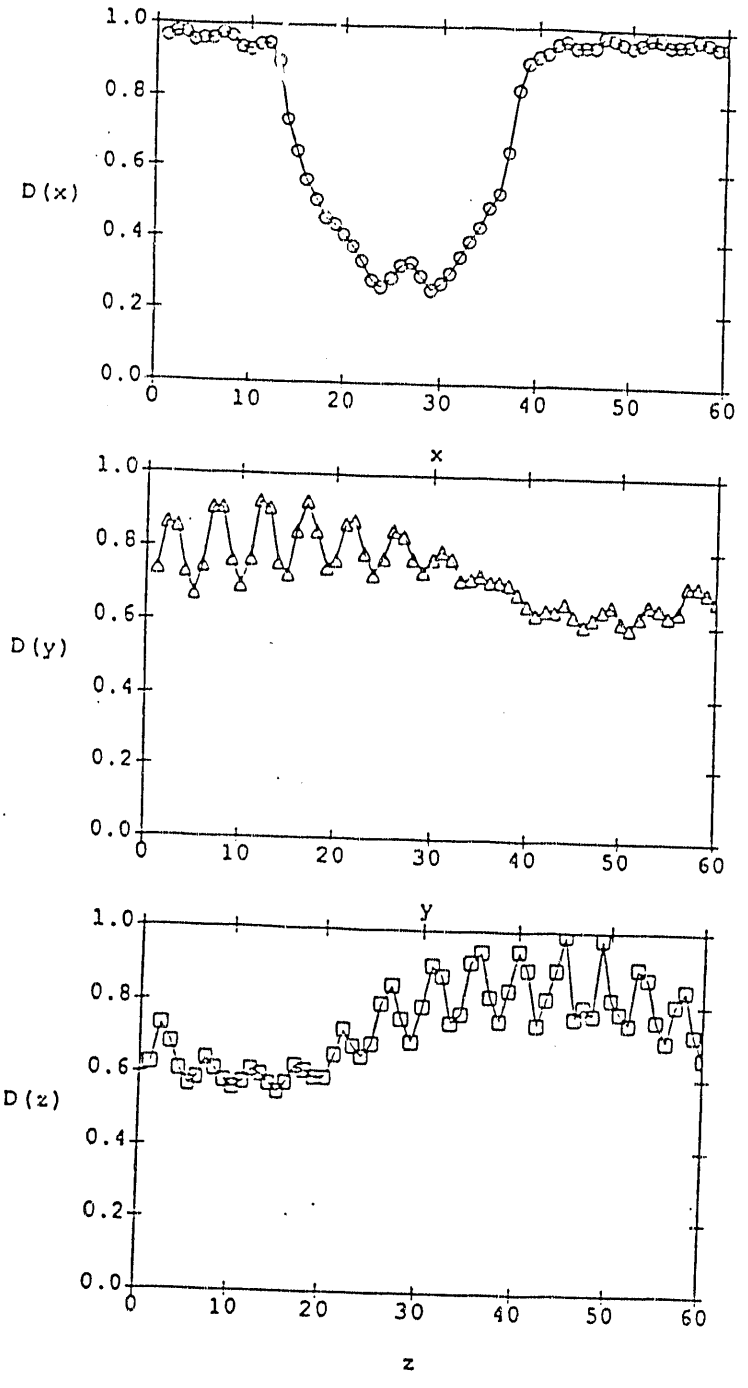


Fig. 10

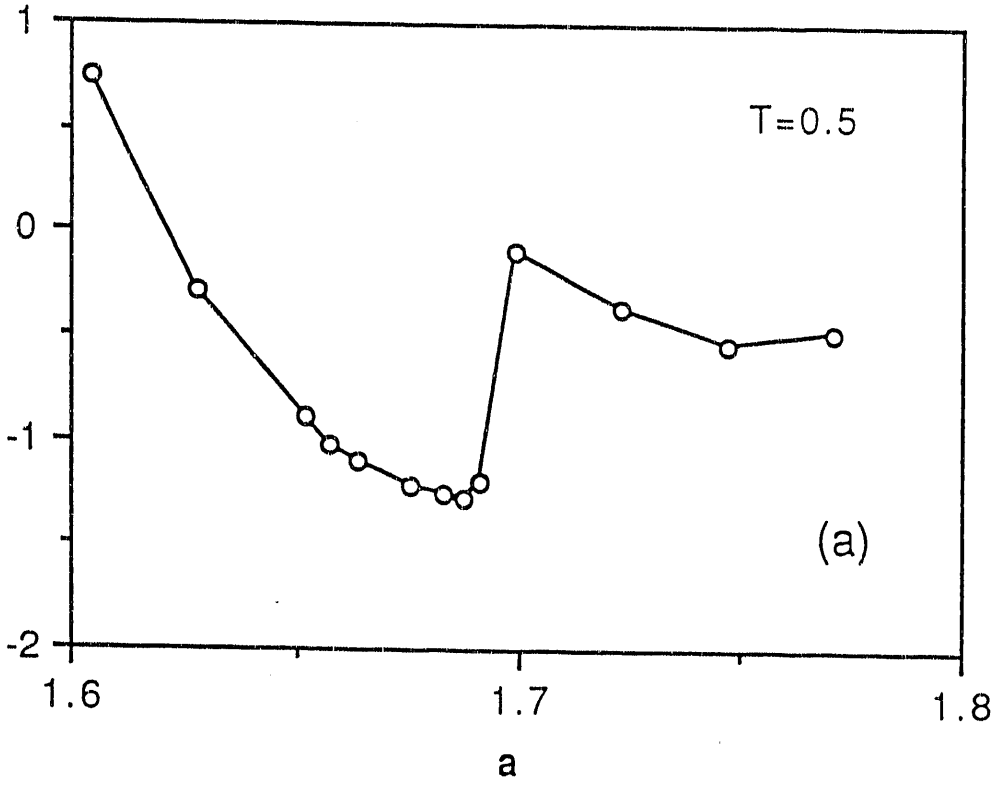


Fig. 11(a)

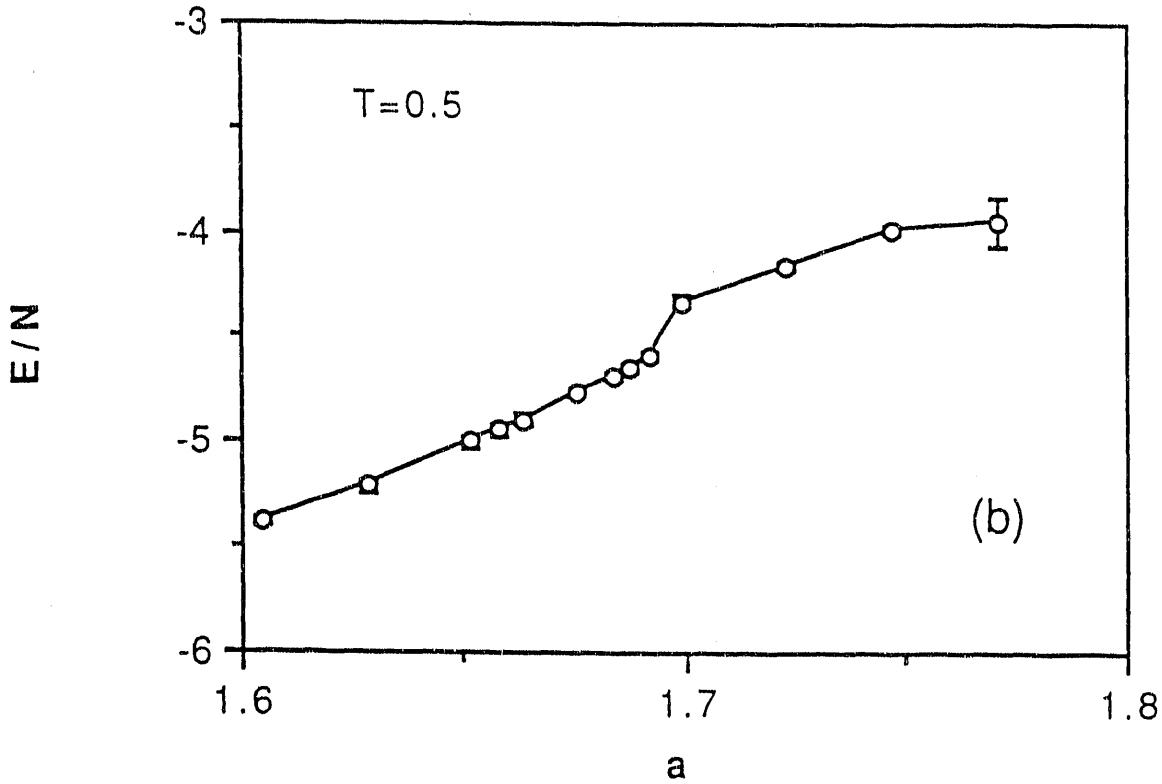


Fig. 11 (b)

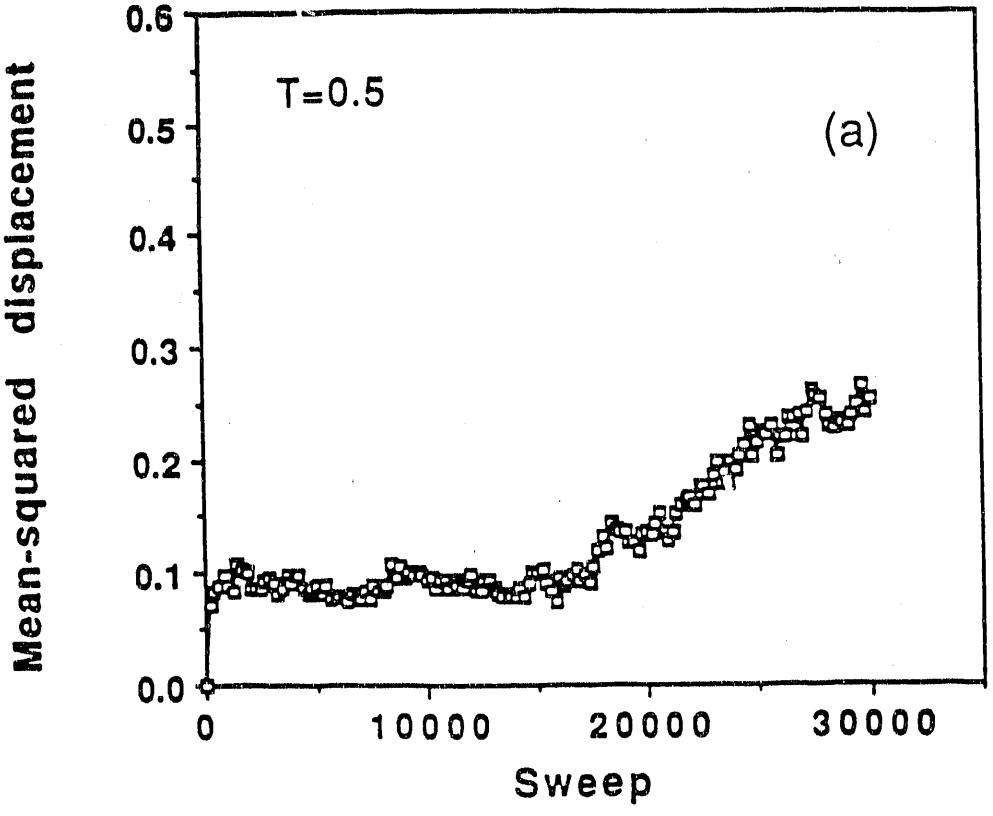
Mean-squared displacement
0.6
0.5
0.4
0.3
0.2
0.1
0.0
T=0.5
(a)
0
10000
20000
30000
Sweep

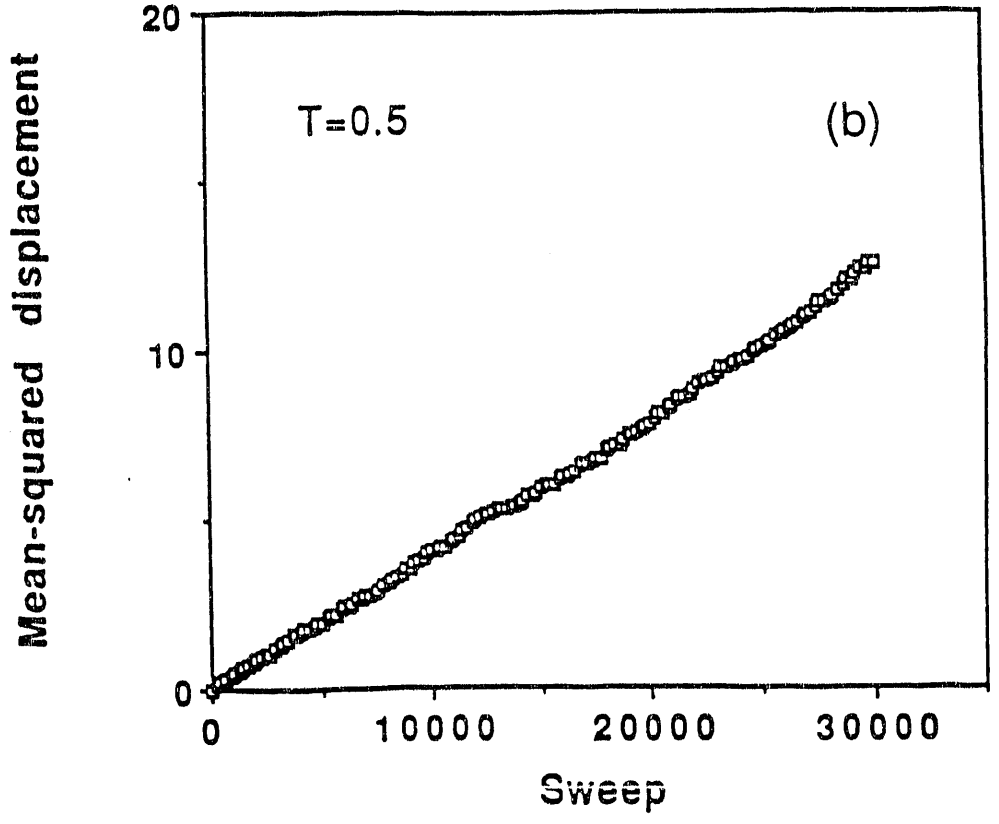
Mean-squared displacement
20
10
0
T=0.5
(b)
0
10000
20000
30000
Sweep

Fig. 12

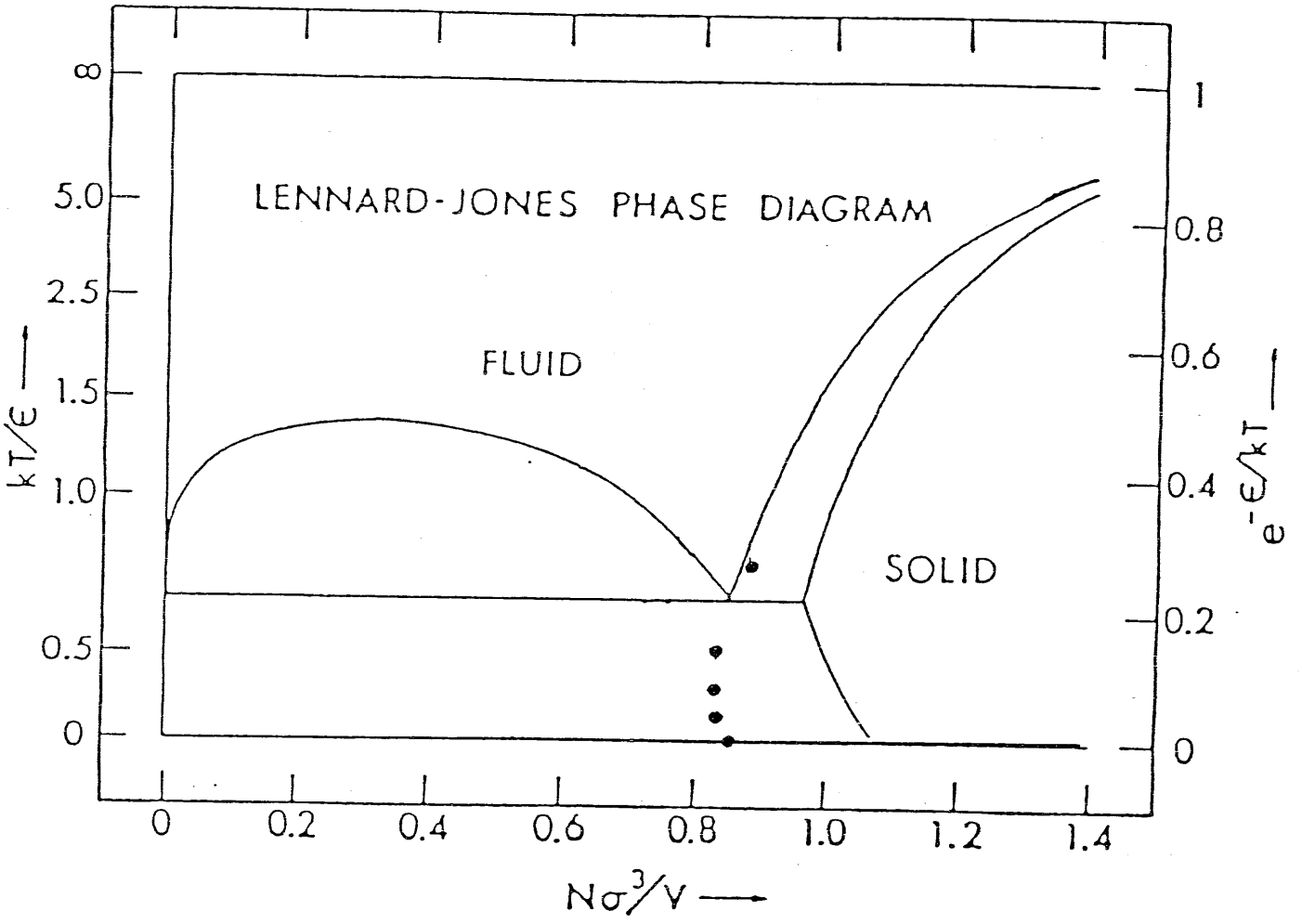
LENNARD-JONES PHASE DIAGRAM
FLUID
SOLID
kT/ε
∞
5.0
2.5
1.5
1.0
0.5
0
0
0.2
0.4
0.6
0.8
1.0
1.2
1.4
Nσ³/V
1
0.8
0.6
0.4
0.2
0
e^-ε/kT

Fig. 13

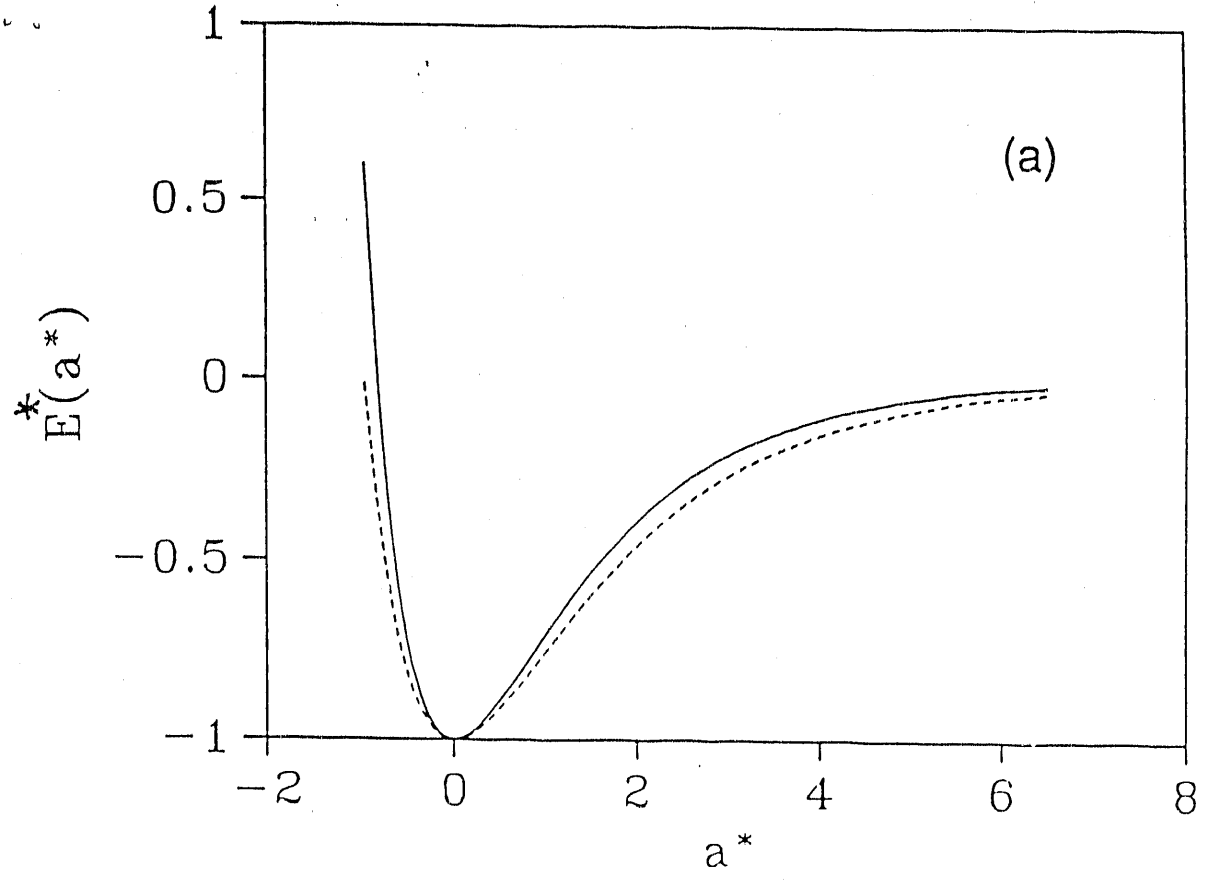


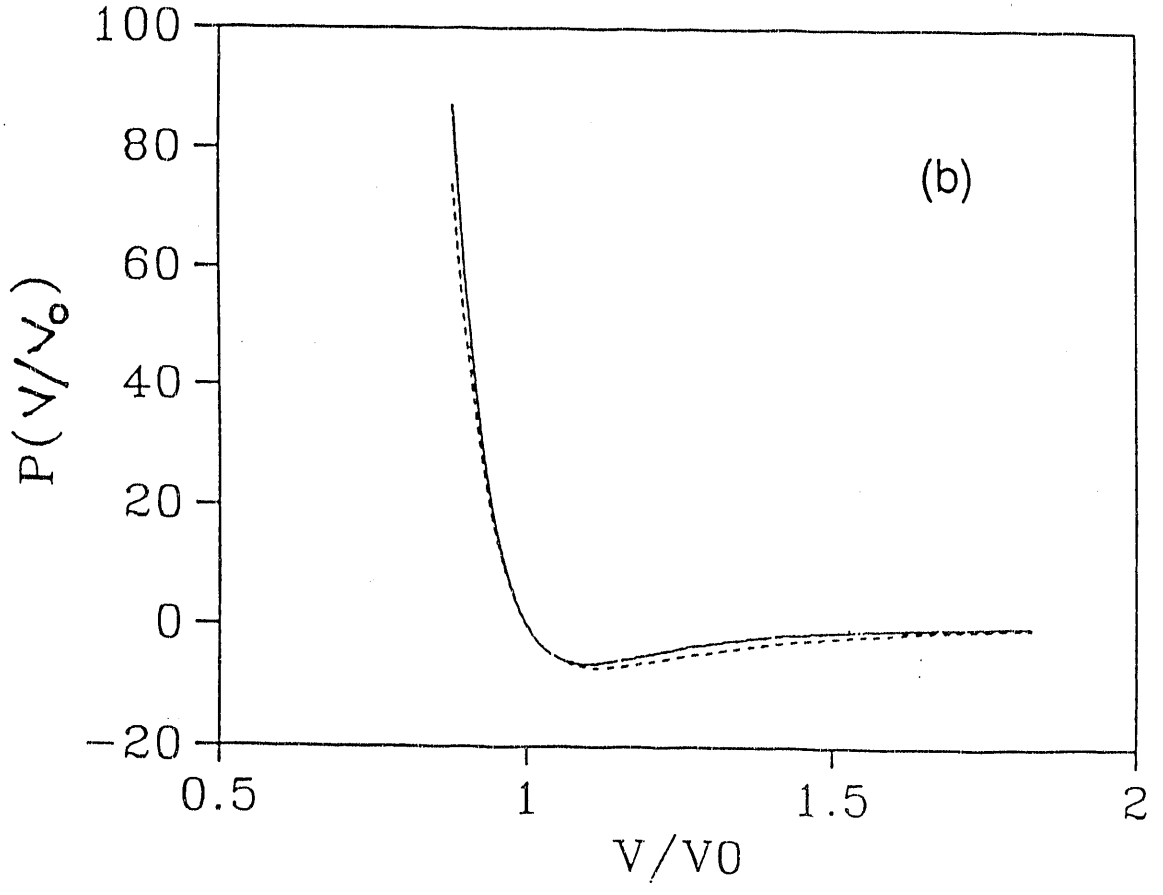


Fig. 14

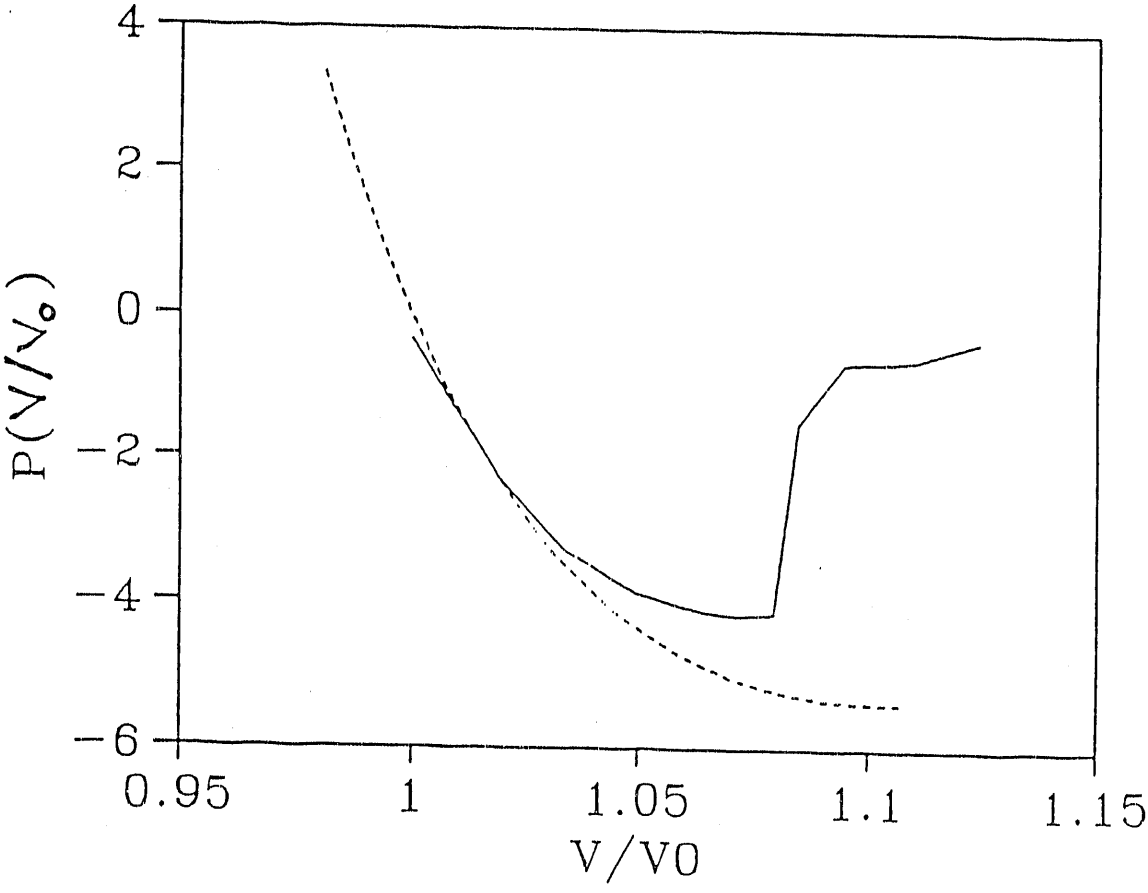


Fig. 15

DATE
FILMED
8/18/92